Vafadar, Farid; Jaaranen, Joonas; Fink, Gerhard

Experimental stiffness investigation of finger joints in glued laminated timber beams using digital image correlation

Published in:
Construction and Building Materials

DOI:
10.1016/j.conbuildmat.2024.137095

Published: 09/08/2024

Document Version
Publisher's PDF, also known as Version of record

Construction and Building Materials 438 (2024) 137095

Contents lists available at ScienceDirect

Construction and Building Materials

journal homepage: www.elsevier.com/locate/conbuildmat

Experimental stiffness investigation of finger joints in glued laminated timber beams using digital image correlation

Farid Vafadar *, Joonas Jaaranen, Gerhard Fink

Aalto University, Department of Civil Engineering, Espoo, Finland

ARTICLE INFO

Keywords:
Finger joints
GLT beams
Stiffness
Digital image correlation
Strain distributions

ABSTRACT

Glued laminated timber (GLT) is an engineered wood product widely used in structural applications. The mechanical properties of the GLT beams significantly depend on the mechanical properties of local weak sections such as knots and finger joints (FJs). Conventionally, the mechanical behavior of the local weak sections has been mainly investigated in the individual lamellae. In the present study, their mechanical behaviors within the GLT beams are investigated. 22 GLT beams with well-known beam setups in four-point bending tests were studied. Digital image correlation was used to measure displacements and strains in the region of the beams with the constant bending moment. This paper presents the strain distributions in the GLT beams and discusses the influence of the timber board arrangements and, accordingly, the knots and the FJs. As expected, the strain distributions of the GLT beams vary significantly. Depending on the arrangement of the knots, they can cause strain concentrations in the beams, which can be distributed to the adjacent lamellae. FJs do not cause significant strain concentrations; however, they can influence the strain distribution along the lamellae. Furthermore, a reduced stiffness of the FJs, compared to the connected timber boards, is identified.

1. Introduction

Glued laminated timber (GLT) is an engineered wood product widely used in structural applications. GLT beams are fabricated of layers of timber boards glued together. Before the fabrication, the timber boards are strength-graded. The graded timber boards are connected with finger joints (FJs) in the longitudinal direction to lamellae, which are cut to the length of the beams. The lamellae are stacked and glued together to fabricate the beams (see, *e.g.*, [1] for a more detailed description of the fabrication process).

The mechanical properties of the GLT beams depend on the mechanical, morphological, and geometrical characteristics of the timber boards and the FJs [2–5]. It is essential to address that the (geometrical) arrangements of the timber boards (and, accordingly, the arrangement of the FJs) influence the mechanical properties of the GLT beams. In [6], the influence of the timber board arrangements in terms of the laminating effect was discussed. The lamination effect was defined as the increase in the strength of lamellae when being bonded in a GLT beam compared to the single lamellae. One of the reasons for the strength increase was found in the reinforcement of the low-stiffness areas by the adjacent lamellae. The reinforcement provides alternative paths for the stresses around the lower stiffness areas. As a result, the capacity of the cross-section will increase. The study emphasized the significance of examining local defects' stiffness concerning the GLT beams' mechanical properties. This perspective aligns with the findings in [7,8], where it was concluded that even a minor reduction in stiffness within small areas, such as knots and FJs, can impact the strength of the GLT beams. Thus, of great importance is to analyze the stiffness properties of the knots and FJs. In the current study, the stiffness properties of FJs, in particular, are addressed, highlighting their significant impact on the mechanical properties of the GLT beams.

Extensive studies have examined the mechanical properties of the FJs in individual lamellae, *e.g.*, [9–13]. Nevertheless, the stiffness properties of the FJs were assessed in the limited studies. In [14], the tensile stiffness of finger-jointed lamellae was investigated and compared to unjointed specimens (serving as control specimens). The modulus of elasticity was measured at the midpoint of the specimens during tensile tests. The results demonstrated a reduction in the mean modulus of elasticity within finger-jointed specimens when contrasted with control specimens. In [15], the study involved quantifying the flat-wise bending stiffness profile at increments of approximately 100 mm along the longitudinal axis of finger-jointed timber boards. Compared to unjointed timber boards, high variability in the stiffness profile along finger-jointed specimens was observed. In [16], the mechanical properties of poplar timber were examined under tension loading, both with and without the presence of FJs in small-scale samples. The

* Corresponding author.
E-mail addresses: farid.vafadarestiar@aalto.fi (F. Vafadar), joonas.jaaranen@aalto.fi (J. Jaaranen), gerhard.fink@aalto.fi (G. Fink).

https://doi.org/10.1016/j.conbuildmat.2024.137095
Received 22 March 2024; Received in revised form 28 May 2024; Accepted 12 June 2024
Available online 21 June 2024

Table 1
Descriptive statistics of E_{dyn} for the timber boards groups. COV stands for coefficient of variation.

Class	Range [MPa]	n [-]	Mean value [MPa]	COV [–]
Rejected	< 9600	50	8706	0.09
T14	9600–12300	104	11 063	0.07
T22	> 12300	57	13 738	0.08

digital image correlation (DIC) method was used to measure the strain distributions. The findings indicated that the existence of FJs reduced the modulus of elasticity in the longitudinal direction up to 24%. The literature above consistently indicates a decrease in the stiffness properties of finger-jointed timber boards compared to unjointed samples. However, the stiffness behavior of FJs and connected timber boards within the GLT beams have not been investigated in detail.

The results of the stiffness investigation can be used to study the relationships between the FJs and the connected timber board stiffness properties. This is essential to developing or updating the FJ stiffness models for estimating the GLT beams' mechanical properties. A few studies have addressed the relationships between the FJ stiffness and the properties of the connected timber board. In [17], a regression model for estimating the FJs tensile stiffness based on the lower value of the connected board's densities was developed. In [18], the FJs' flatwise three-point bending stiffness was estimated based on the stiffness of the connected timber boards. The specimen's cross-section dimensions were $w \times t = 152 \times 50$ mm^2. The stiffness was measured for the spans with a length of approximately 610 mm connected timber board segments and 610 mm segment with the FJ in the center. Therefore, the stiffness properties indicated relatively global characteristics. A strong correlation was found between the FJ stiffness and the average stiffness of the connected timber boards. Because of this strong correlation, in [6], it was speculated that little stress redistribution takes place around the FJs within the GLT beams. Moreover, in [19], it is assumed that the FJ stiffness is the average value of the connected timber board stiffnesses for developing the mechanical properties of the GLT beam prediction model. Nonetheless, the relationships between the stiffness properties of FJs and the connected timber boards within the GLT beams have not been studied locally.

The present study investigates the stiffness properties of the FJs within the GLT beams and their relationship with the connected timber board properties. The experimental investigations on 22 GLT beams with lengths of 5 meters are presented. The DIC method is used to measure the displacements and strains in the areas of the beams with the constant bending moment. The method has been adopted to study the strain distributions and mechanical properties of the local defects in the literature [20–23]. In those studies, the DIC method demonstrated its suitability for measuring the strains and providing insights into timber structures' mechanical behavior (*i.e.*, strain distributions) under various loading conditions. In the current paper, the method is used to analyze the influence of the timber board arrangements accordingly knots and FJs on the mechanical behavior of the GLT beams locally.

2. Materials and methods

The experimental investigations were performed on 22 GLT beams ($b \times h \times l = 115 \times 270 \times 5000$ mm^3). This section introduces the fabrication process and the specifications of the GLT beams, the experimental setups, and the test procedure. Also, an overview of the DIC measurement and the validation procedures is discussed.

2.1. Specimens

In total, 211 Spruce timber boards ($w \times t = 125 \times 50$ mm^2 with lengths between 3800 mm and 4700 mm) from southern Finland were used to fabricate the GLT beams. The timber boards were investigated using two commercial grading devices: Precigrader [24] and Finscan [25]. The first one measures the dynamic modulus of elasticity (E_{dyn}) based on the eigenfrequency of each timber board. Based on the information from Precigrader, the timber boards were classified into three groups: Rejected, T14, and T22 [26]. Descriptive statistics of every group are mentioned in Table 1. The second grading device (Finscan) was only used to measure the knot information of every timber board.

The grading information of each timber board from the Precigrader and Finscan devices was stored and tracked through the fabrication process of the beams to identify the local material properties within the beams. The arrangement of timber boards in GLT beams was random, meaning that in every GLT beam, all three timber board classes (Rejected, T14, and T22) could be found.[1] The setup for each beam is known, *i.e.*, the timber board's position and E_{dyn}, the position of the FJs, as well as the size and position of each knot, are known.

Based on the Finscan data (dimensions and coordinates of the knots), a knot parameter was calculated. For this study, the projected knot area ratio was used, which represents the ratio of the projected cross-sectional areas of knots within a predefined length (overlapping knots were accounted for only once) to the cross-sectional area of the timber boards. Generally, a length of 150 mm is used (see, *e.g.*, total knot area ratio tKAR in [27]). However, in this study, in order to illustrate the influence of local defects, a short length of 10 mm was adopted (KAR_{10}). The layup of one GLT beam is exemplarily illustrated in Fig. 1.

The profile of the FJs, including the length of the fingers, pitch, and width of the cutter, were 15, 3.8, and 0.42 mm, respectively, according to EN15497 [28]. Melamine Formaldehyde adhesive was used to produce the FJs. There were six lamellae in every GLT beam, and all the lamellae had the same thickness, equal to 45 mm.

2.2. Experimental setup and procedure

The experimental investigation of the GLT beams took place at the structural laboratory of the Department of Civil Engineering at Aalto University. The beams were conditioned in a climate chamber at 20 °C, with a relative humidity of 65%, and the beams' mass was recorded before testing.

The beams were tested in four-point bending according to EN408 [29] (Fig. 2). The load was applied using a hydraulic cylinder and a load balancer to distribute the force evenly at two points. The testing protocol was force control with a 10 kN/min loading rate.

Local and global deformations were measured with two linear variable differential transformers (LVDT). Only one LVDT on the opposite side was installed to measure the local deformation because of the DIC measurements. The LVDT was removed at 40% of the estimated ultimate force to prevent damage during failure.

2.3. DIC measurements

The DIC method was used to measure displacements and strains of the GLT beams; [30] was chosen as a primary reference for designing the DIC measurements. The DIC measurement setup is shown in Figure 3. The dimension of the region of interest (2000 × 270 mm) was chosen to cover the beams' region with the constant bending moment (Fig. 3a). Two cameras (resolution: 4000 × 2000 pixels, focal length: 16 mm) oriented at a stereo-angle (approx. 25°) were used (Fig. 3b,c). The cameras were positioned approximately 2300 mm from the GLT beams.

[1] It was planned to fabricate homogeneous GLT beams in two strength classes GL24 h and GL30 h. However, the timber boards were mixed due to a technical error.

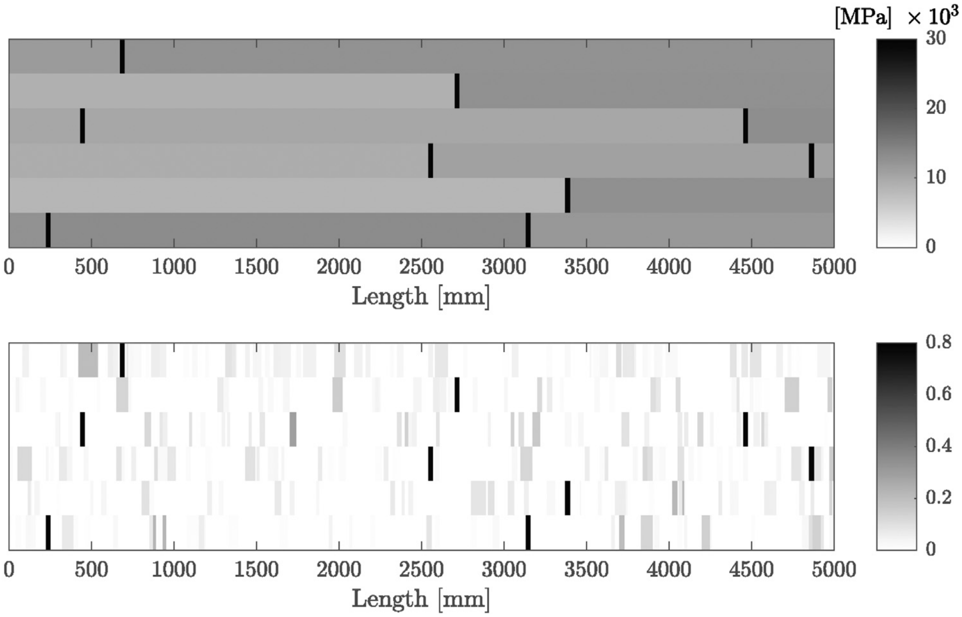

Fig. 1. E_{dyn} (top) and KAR_{10} values (bottom) maps of each timber board in beam no. 6. The thick vertical black lines indicate the FJs.

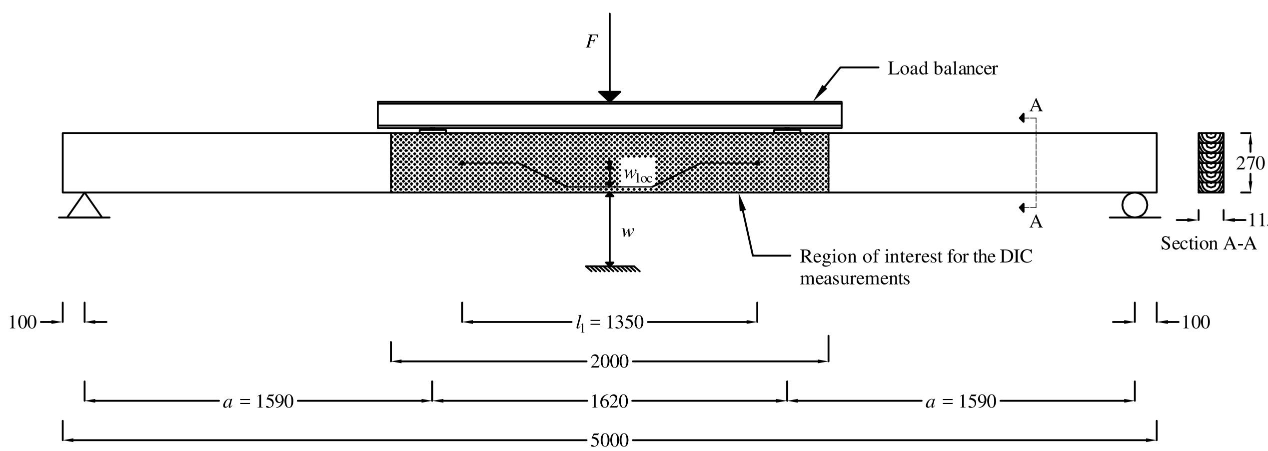

Fig. 2. Schematic illustration of the test setup in accordance with EN408 [29], dimensions in (mm).

Three light-emitting diodes (LED) were used to provide the suitable brightness (Fig. 3d).

A novel contrast pattern with a feature of a speckle pattern of approximately three pixels was applied in the region of interest (Fig. 3e). The pattern enabled evenly-spaced features with varying shapes within the desired size range and consistent information from the whole region of interest. For more detailed information about the pattern features, see [31,32], and for its applications on wooden specimens, see [33].

Calibration images were captured before the tests. Digital images were taken during the experiments at the rate of two frames per second. For image correlation, a subset size of 27 pixels, a step size of 7 pixels, and a filter size of 11 pixels were chosen based on the virtual strain gauge study. The image of the sample in the unloaded state was considered the reference image for the correlation analysis. A commercial image acquisition software, VIC-SNAP version 9, was used to capture calibration and beam images [34], and digital image correlation software, VIC-3D version 9.4.26, was adopted to perform calibration and correlation analysis [35].

2.4. Validation of the DIC measurements

The DIC measurements were validated by two methods: checking the epipolar error (or projection error), and comparing to the LVDT measurements. The epipolar error is a metric to indicate possible drift, misalignment, or vibrations in the stereo-DIC camera and lens systems score [30]. The epipolar error for each beam was on the order of the calibration score, which indicates no significant error in the DIC measurements.

The global bending stiffness ($E_{m,g}$) and the vertical deflection of the point in the middle of the GLT beams from the DIC and LVDT measurements were compared (Fig. 4). The stiffnesses were calculated according to EN408 [29], and the deflections were considered at 90% of the ultimate loads ($w_{0.9F_u}$) to eliminate the deflections due to delaminations or cracks on the side surface. There is a comprehensive agreement between DIC and LVDT measurements with a correlation coefficient $r \geq 0.99$. Thus, The DIC measurements were reliable for the strain investigations in the GLT beams.

3. Mechanical properties and failure types

In this section, the mechanical properties and the failure types of the GLT beams are investigated. The bending test results are summarized in

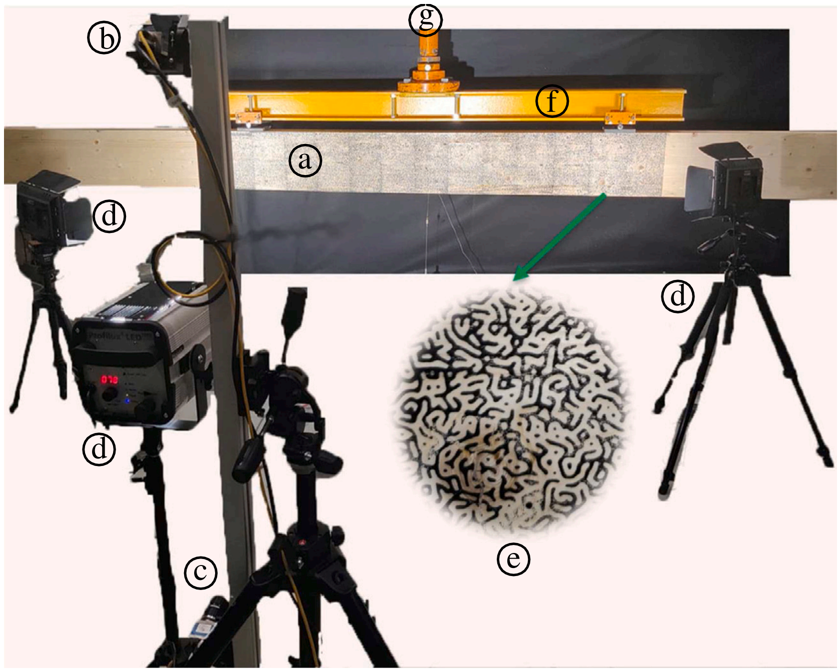

Fig. 3. Test and DIC measurement setup, (a) region of interest, (b) camera 1, (c) camera 2, (d) LEDs, (e) speckle patterns, (f) load balancer, (g) loading cylinder.

Table 2
Four-point bending test results of the GLT beams.

ID	F_u [a]	f_m	$E_{m,g}$ [b]	$E_{m,g,G}$ [c]	$E_{m,l}$	ρ [d]	Failure type	
	[kN]	[MPa]	[MPa]	[MPa]	[MPa]	[kg/m^3]	lowest lamella	2nd lowest lamella
1	60.6	34.5	10 550	11 084	11 612	454	FJ	FJ
2	62.5	35.6	10 357	10 870	–	435	KC	KC
3	57.4	32.6	10 325	10 835	11 949	436	KC/FJ	KC
4	46.6	26.5	9470	9898	10 071	431	KC/FJ	CW
5	62.4	35.5	11 334	11 951	12 781	450	KC	–
6	51.1	29.0	10 968	11 545	11 752	447	FJ	CW
7	61.5	35.0	10 669	11 214	12 455	435	FJ	FJ
8	68.0	38.6	11 375	11 998	12 229	452	FJ	FJ
9	63.7	36.2	9399	9820	10 727	448	KC	CW
10	68.6	39.0	10 042	10 524	10 294	438	FJ	CW
11	56.2	32.0	9567	10 003	10 092	450	KC	KC
12	42.5	24.2	11 839	12 515	14 139	488	FJ	–
13	47.3	26.9	8906	9283	9920	456	FJ	CW
14	59.0	33.5	10 337	10 849	10 504	441	KC	KC
15	49.8	28.3	10 497	11 024	13 283	450	KC	CW
16	55.1	31.3	10 644	11 187	12 193	453	FJ	KC
17	46.7	26.6	11 376	11 999	12 970	458	KC/FJ	CW
18	55.8	31.7	10 527	11 058	11 037	456	KC	KC
19	53.6	30.5	10 156	10 649	11 402	454	KC	KC
20	58.8	33.5	8694	9053	9000	450	KC	CW
21	64.2	36.5	10 963	11 540	12 027	450	FJ	FJ
22	62.3	35.4	11 049	11 635	12 729	454	KC/FJ	FJ
Mean value	57.0	32.4	10 411	10 933	11 579	449	–	–
COV	0.12	0.12	0.07	0.08	0.11	0.02	–	–

[a] F_u is the maximum force up to beam failure.
[b] $E_{m,g}$ is the global bending stiffness without shear deformation correction by taking shear modulus (G) infinite.
[c] $E_{m,g,G}$ is the global bending stiffness with shear deformation correction by taking $G = 650$ MPa.
[d] ρ is the density, which is calculated by dividing the beam's mass by its volume.

Table 2. The bending strength (f_m), and stiffnesses (E_m) are calculated based on EN408 [29]. The strength and stiffness of the beams are compared to the conventional GLT beam strength classes. The cumulative lognormal distribution functions for the bending strengths and the local bending stiffness ($E_{m,l}$) from the test results and for GL24h to GL30h strength classes (for the mechanical properties of each strength class, see EN14080 [36]) are shown in Fig. 5. The probability distribution parameters (mean and standard deviation) for the GLT beam strength classes are calculated based on the COV values for the bending strength and the stiffness in JCSS [37]. The COV for the bending strength and the stiffness of 0.15 and 0.13 are considered, respectively. Although there is an alignment between the probability distribution functions of the test results and of the GLT beam strength classes, it is important to highlight that the COV values mentioned in JCSS account for both within and between batches variabilities. Nevertheless, the test results exclusively address within-batch variabilities. The COV values from the test result are compared with the values based on the previous studies from GLT beams fabricated from graded timber boards (based on the summary

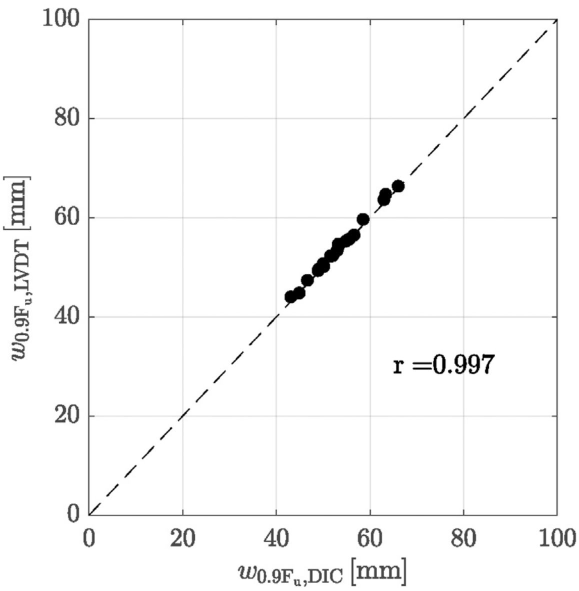

Fig. 4. Global deflection of the GLT beams at the 90% of the ultimate loads based on the DIC and the LVDT measurements.

presented in [38]). The variation of the bending strength is within the range of previous research, while the variation of the bending stiffness is larger.

Correlation analyses are conducted between various mechanical properties (f_m, $E_{m,l}$, ρ). The analysis was affected by one outlier (beam no. 12). Overall, no strong correlation could be identified between the properties.

The failure types in the two lowest lamellae of the GLT beams are identified (following the method mentioned in [5]) as:

- Knot cluster failure (KC): the failure happened within knot clusters; see Fig. 6(a).
- FJ failure (FJ): the failure happened within the FJs; see Fig. 6(b).
- Clear wood failure (CW): the failure happened within the clear wood section.

About half of the GLT beams failed in knot clusters or FJ, respectively. In four GLT beams, the failure could not be clearly associated with one failure mode (denoted as KC/FJ). A comparison between the GLT beams that failed in the KC and those that failed in the FJ did not indicate significant differences in the bending strength.

4. Strain distributions within GLT beams

The strain distributions in the GLT beams exhibit considerable variation, influenced by variations in the stiffness properties of timber boards and the presence of knots and FJs. This section presents a qualitative overview of the longitudinal strain distributions (ε_{xx}) in the GLT beams and their relationships to the timber boards properties (the E_{dyn}, and especially the KAR_{10} values) and their arrangements. The E_{dyn}, KAR_{10}, and ε_{xx} (at 60% of the maximal load) of the GLT beams are summarized in Appendix.

4.1. Influence of the E_{dyn} variation

The influence of variation in the timber boards E_{dyn}, on the ε_{xx} is investigated. Connecting two timber boards with notable stiffness disparities through finger jointing can lead to significant fluctuations in ε_{xx}. For instance, in the topmost lamella of beam no. 15, distinct compression strains in the timber board on the left side of the FJ are evident compared to the right. This discrepancy can be attributed to differences in the dynamic modulus of elasticity between the two timber boards: $E_{dyn,Left}$ = 9000 MPa, $E_{dyn,Right}$ = 17100 MPa. A similar trend is observed in the topmost lamella of beam no. 20. In this case $E_{dyn,Left}$ = 7200 MPa while $E_{dyn,Right}$ = 13 300 MPa.

4.2. Influence of the knots

Knots can significantly impact the variation of ε_{xx} depending on their arrangements within the GLT beams. For example, in the two lowest lamellae of beam no. 19 (at 2000–2100 mm), there is a significant strain concentration attributed to the accumulation of knots in those lamellae.

The strain concentrations induced by knots can extend to the neighboring lamellae and fluctuate the strain distributions over the beam height and along the lamellae. For instance, in Fig. 7, the strain distributions over the height of beam no. 10 are shown for two sections (A-A and B-B) at different load levels; $0.4F_u$ and $0.8F_u$. The sections are obtained from the same timber boards in all lamellae without any FJs between the two sections. Section A-A includes all the lamellae (1 to 6) consisting of clear wood, indicating no knots with a $KAR_{10} \geq 0.1$. In this section, the strains are approximately linearly distributed over the beam height, with maximum absolute values of the strains occurring in the outermost fibers in the tension and compression zones. Section B-B comprises knots in the tension and compression zones, resulting in non-linear strain distribution. Because of the knots, the maximum strains occur in lamellae 2 and 5.

The relationship between the strain distributions and the KAR_{10} values is studied. The notable KAR_{10} values align with corresponding strain concentrations. The differences between the DIC measurements and the KAR_{10} can be attributed to the DIC method's sensitivity to surface defects. For example, the strain concentrations may occur despite the marginal KAR_{10} values. This is evident in beam no. 18, where the lowest lamella between 2700–2800 mm displays strain concentrations resulting from surface knots.

4.3. Influence of the FJs

The influence of the FJs on the strain distributions over the beam height and along the lamellae is investigated. Overall, the FJs exhibit no significant strain concentrations compared to the clear wood of connected timber boards, with the strains approximately linearly distributed over the beam height. However, notable strain concentrations may arise for the FJs situated in the lower lamellae. It should be noted that significant strain concentrations were identified only in FJ with indications of lower quality, such as irregular finger arrangement (*e.g.*, beam no. 6) or the presence of knots (*e.g.*, beam no. 22).

Along the lamellae, the FJs fluctuate strain distributions, particularly in the outermost lamellae, indicating variation in stiffness properties. One example is illustrated in Fig. 8. The central 50 mm is designated as the FJ zone, and the 100 mm on each side represents the clear wood of the connected timber board zones. The strains in the timber board on the left side of the FJ are higher than the strains on the right. This is expected since $E_{dyn,Left}$ = 9400 MPa while $E_{dyn,Right}$ = 12 100 MPa. There is a transition in the strain values in the FJ zone, and the strains become more uniform in distant regions of the FJ. In the next section, the stiffness properties of the FJs are investigated quantitatively.

5. Stiffness analysis of the FJs and the connected timber boards within the GLT beams

The stiffness properties of the FJs and the connected timber boards located in the two outmost lamellae (see Fig. 7 for the numbering order of the lamellae) are investigated. Only knot-free samples with a $KAR_{10} \leq 0.1$ are considered for the analysis. For the investigation, the apparent stiffnesses of the FJs (E^*_{FJ}) are compared to those of

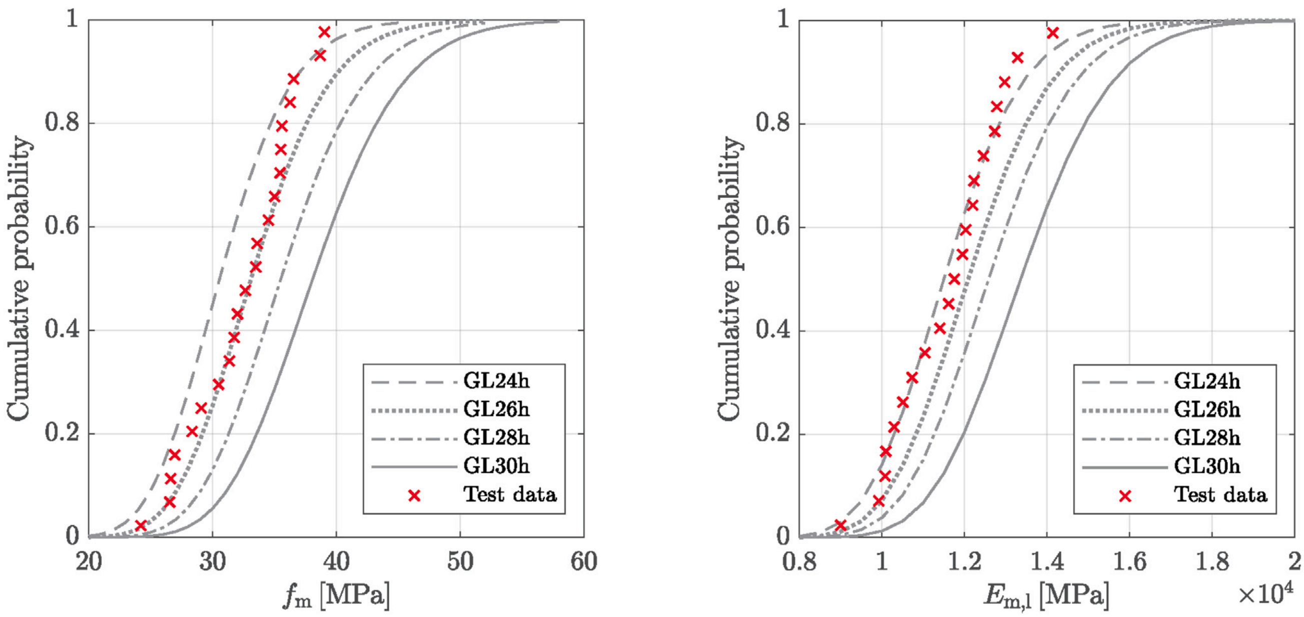

Fig. 5. Cumulative probability of the material properties for GL24h, GL26h, GL28h and GL30h strength classes based on EN14080 [36], JCSS [37], and test data, left: bending strength (f_{m}), right: local bending stiffness ($E_{\mathrm{m,l}}$).

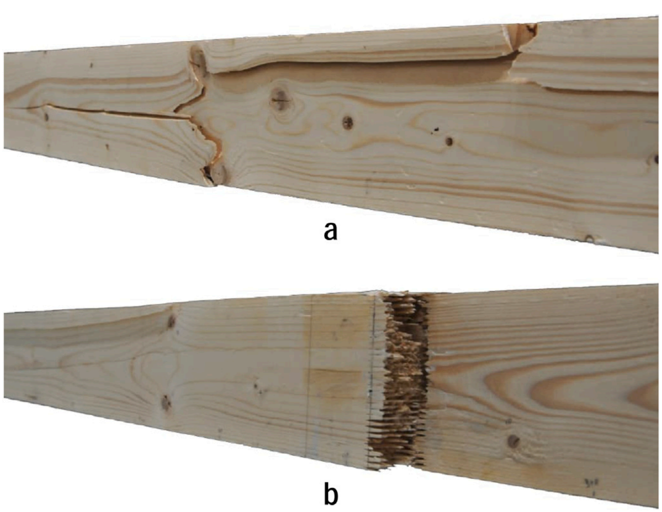

Fig. 6. Examples of typical failure types in the lowest lamellae of the GLT beams. (a) knot cluster failure, (b) FJ failure.

the connected timber boards (E^*_{tb1} and E^*_{tb2}). The apparent stiffness properties are calculated according to Eq. (1), which is based on the apparent bending stresses (σ^*) and the average longitudinal strains ($\varepsilon_{\mathrm{xx}}$). Consideration of the apparent term for the stiffness properties and the bending stresses arises from the impracticality of applying conventional beam theory for calculating actual stresses as well as stiffnesses in the local weak sections of the GLT beams. This might be attributed to variation in the strain distributions (as discussed in Section 4) yet ensures a comparability between the results.

$$E^* = \frac{\Delta\sigma^*}{|\Delta\varepsilon_{\mathrm{xx}}|} \quad \text{with} \quad \sigma^* = \frac{M \cdot y}{I} = \frac{F \cdot a \cdot y}{2I} \tag{1}$$

Where:

- E^* is the apparent stiffness, in [MPa].
- σ^* is the apparent bending stress (from the test results) in [MPa].
- $\varepsilon_{\mathrm{xx}}$ is the average longitudinal strain (from the DIC measurements) within the specific rectangular areas. These areas have a height equivalent to the lamellae (45 mm) and lengths of 50 mm in the FJ zone and 100 mm in the connected board's zone as it is shown in Fig. 9.
- M is the bending moment at the section of interest in [Nmm].
- y is the distance between the middle plane of the GLT beams and the middle of the lamellae in [mm].
- I is the second moment of inertia of the beam's cross-sections in [mm^4].
- F is the applied force in [N].
- a is the distance between a loading point and the nearest support in [mm].

Stiffness calculations are performed using a similar method outlined for stiffness in EN408 [29]. An example of the apparent stress versus average longitudinal strain graphs for the FJ and the connected timber boards is shown in Fig. 10. The range between $0.1F_{\mathrm{u}}$ to $0.4F_{\mathrm{u}}$ is used for the regression analysis; only samples with a correlation coefficient $r \geq 0.9$ are considered.

In total, the stiffness properties of 18 FJs (15 in the tension zone and 3 in the compression zone) are calculated. The apparent stiffnesses (E^*_{FJ} and E^*_{tb}) are shown in Fig. 11. In all of the samples, a reduced stiffness in the area of the FJ could be identified ($E^*_{\mathrm{FJ}} \leq \mathrm{mean}(E^*_{\mathrm{tb1}}, E^*_{\mathrm{tb2}})$). In most of the samples, the FJ stiffness was even smaller than the one of the weaker timber board ($E^*_{\mathrm{FJ}} \leq \min(E^*_{\mathrm{tb1}}, E^*_{\mathrm{tb2}})$). No significant correlation is found between the failure location and the lower E^*_{FJ}. The stiffness property of the FJ in lamella 1 in beam no. 6 is significantly lower than the connected timber boards, and the beam failed in the FJ. As mentioned in the previous section, this could be due to the low FJ quality.

To compare the stiffness properties of the FJs with those of the connected timber boards, the ratios between the FJ stiffness property and the mean ($E^*_{\mathrm{mean}} = \mathrm{mean}(E^*_{\mathrm{tb1}}, E^*_{\mathrm{tb2}})$) and the minimum ($E^*_{\mathrm{min}} = \min(E^*_{\mathrm{tb1}}, E^*_{\mathrm{tb2}})$) values of the connected timber boards are calculated. These ratios are denoted as ($E^*_{\mathrm{FJ}}/E^*_{\mathrm{mean}}$), and ($E^*_{\mathrm{FJ}}/E^*_{\mathrm{min}}$), respectively.

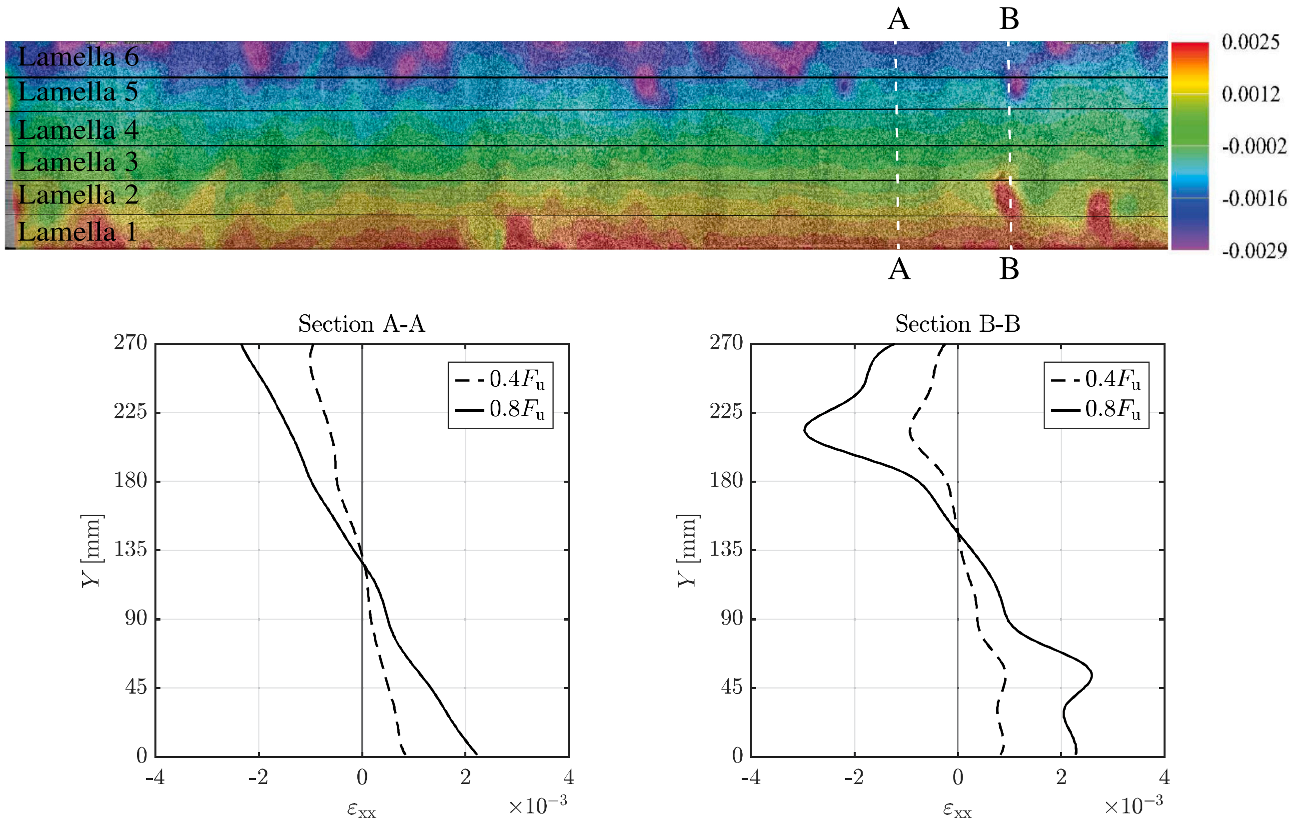

Fig. 7. Longitudinal strain (ε_{xx}) distribution in the region of interest in beam no. 10. The DIC measurements indicate strains at $0.8F_u$, and the horizontal black lines show the edge of each lamella.

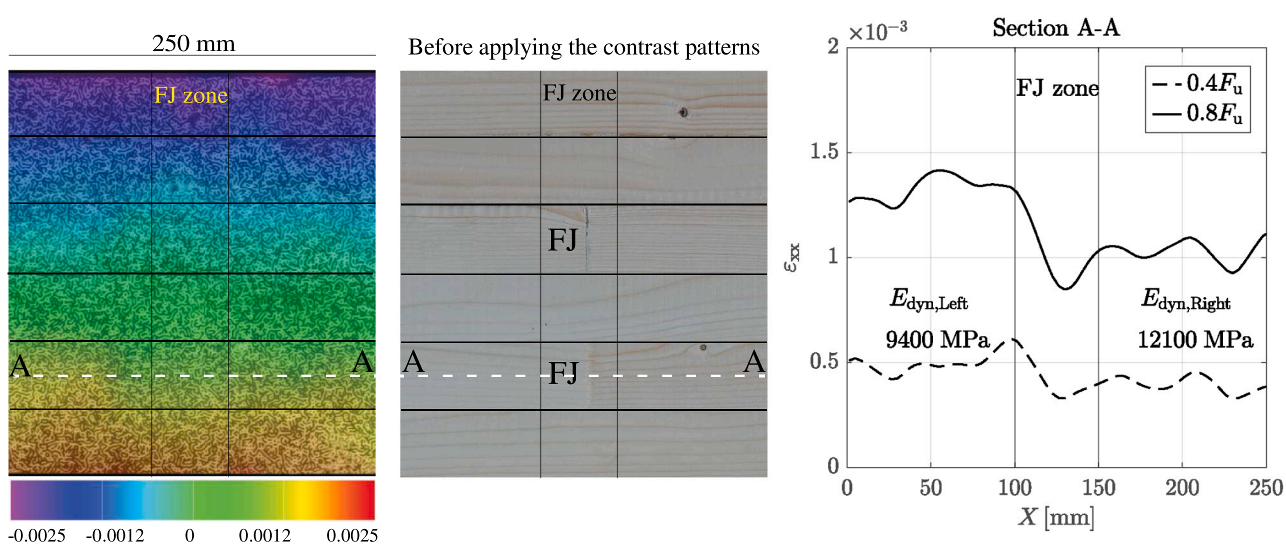

Fig. 8. Longitudinal strain (ε_{xx}) distribution along the lamella and through the FJ in beam no. 21 between 2000–2300 mm (see Appendix). The DIC measurements indicate strains at $0.8F_u$, and the horizontal black lines show the edge of each lamella.

By comparing the mean values of the ratios, it can be said that on average, E^*_{FJ} is 15% smaller than E^*_{mean} and it is 8% smaller than E^*_{min}. Consequently, it can be inferred that there is a reduction in E^*_{FJ} compared to connected timber boards stiffness properties. It should be noted that in individual GLT beams timber boards from different classes were used (see Section 2.1). Therefore, the difference between the dynamic modulus of elasticity of the connected boards is larger compared to a standard procedure. However, it is expected that the main conclusions are not affected.

6. Conclusion and outlook

This research contributes to understanding the stiffness properties of the FJs in the GLT beams locally. In total, 22 GLT beams on a structural scale (5 meters long) with a well-known setup were tested in four-point bending. The displacements and strains in the GLT beams were measured using the DIC method.

The strain distributions in the GLT beams vary significantly due to the random arrangement of knots and FJs and large variations in the knot characteristics. Knots can cause strain concentration; in

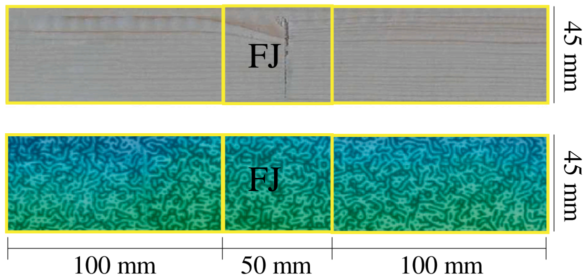

Fig. 9. An example of strain averaging areas for stiffness investigation. The FJ in lamella 4 of beam no. 21 is in the middle of 50 mm long span. The legend for the DIC measurements is shown in Fig. 8.

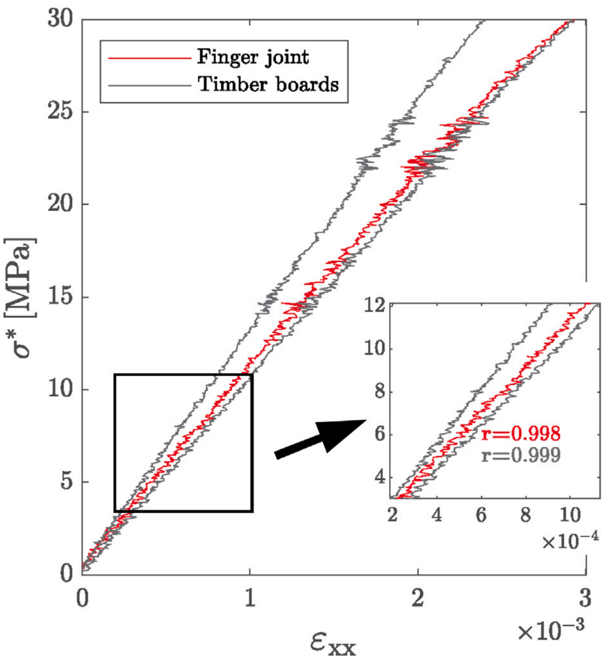

Fig. 10. Apparent stress (σ^*) versus average longitudinal strain (ε_{xx}) for the FJ and the connected boards in beam no. 21. The range is magnified between $0.1F_u$ and $0.4F_u$. The correlation coefficients of connected boards are the same.

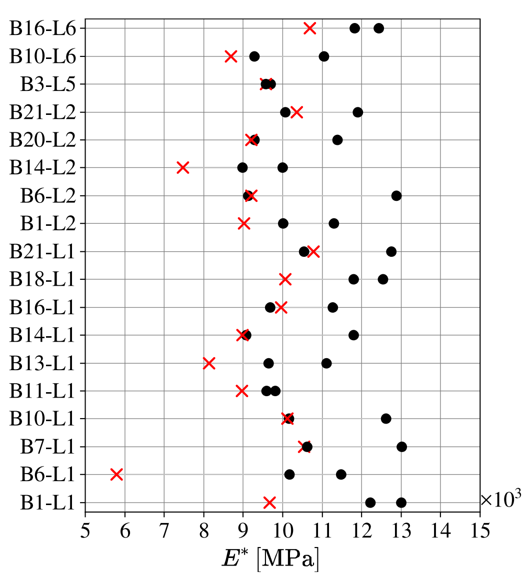

Fig. 11. Apparent stiffness (E^*) of the FJs (red crosses) and connected timber boards (black dots) located in the specific beam (B) and lamella (L).

some cases, the concentration can affect the strain distributions in the adjacent lamellae. The influence of knots on the strain distributions depends on their size and location in the beam and the lamellae.

FJs exhibit more homogeneous mechanical behavior over the height of the beams, which means that strain concentration at the FJ location is not observed compared to the strain distributions at the clear wood of the connected timber boards. However, along individual lamellae in the beams, FJs cause strain fluctuations.

According to the results, the stiffness properties of the FJs are smaller than the mean value of the connected timber boards. On average, the FJs' stiffness properties are 15% lower than the mean value of the connected timber boards and 8% lower than the minimum of the boards. The reduction in the stiffness properties in the FJs can affect the beam strength. The reinforcement of the adjacent lamellae around the FJs provides alternative paths for the stresses to flow; thus, the strength of the whole cross-section will increase, as was discussed in Section 1.

This research can serve as the base for developing or updating the FJ stiffness model in the GLT beams mechanical properties prediction models. In future research, the DIC method can be used as an effective measurement tool to quantify the effect of the knot characteristics, *e.g.*, size, location, direction, and type of knots, on strain distributions in the adjacent lamellae and, accordingly, the mechanical properties of the GLT beams.

CRediT authorship contribution statement

Farid Vafadar: Writing – review & editing, Writing – original draft, Visualization, Methodology, Investigation, Formal analysis, Data curation, Conceptualization. **Joonas Jaaranen:** Writing – review & editing, Methodology, Conceptualization. **Gerhard Fink:** Writing – review & editing, Supervision, Project administration, Funding acquisition, Conceptualization.

Declaration of competing interest

The authors declare the following financial interests/personal relationships which may be considered as potential competing interests: Gerhard Fink reports financial support was provided by Academy of Finland. If there are other authors, they declare that they have no known competing financial interests or personal relationships that could have appeared to influence the work reported in this paper.

Data availability

Data will be made available on request.

Acknowledgments

This research has been conducted with funding from the Academy of Finland (decision no. 13334004). The authors thank Versowood Group Oy and Microtec for their support and cooperation during specimen fabrication and transportation.

Appendix

In this appendix, the E_{dyn}, KAR_{10}, and DIC measurements of the region of interest in the GLT beams are shown (see Figs. 12–31). The DIC measurements belong to the 60% Fu load level. Beam no. 2 (Fig. 13) was used to optimize the DIC parameters, which is why the results may not be consistent with other beams. It should be noted that the digital images of two beams (numbers 12 and 17) are missing because of an error in the storage system.

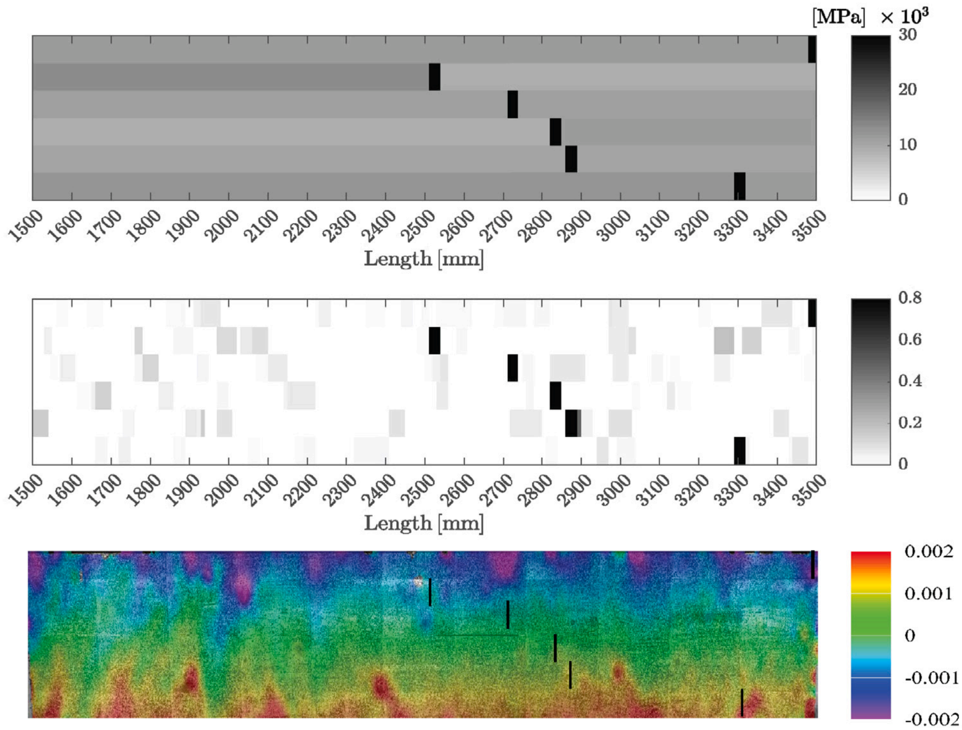

Fig. 12. E_{dyn} (top), KAR_{10} values (middle), and ε_{xx} (bottom) in the region of interest in beam no. 1. Black lines indicate the FJs.

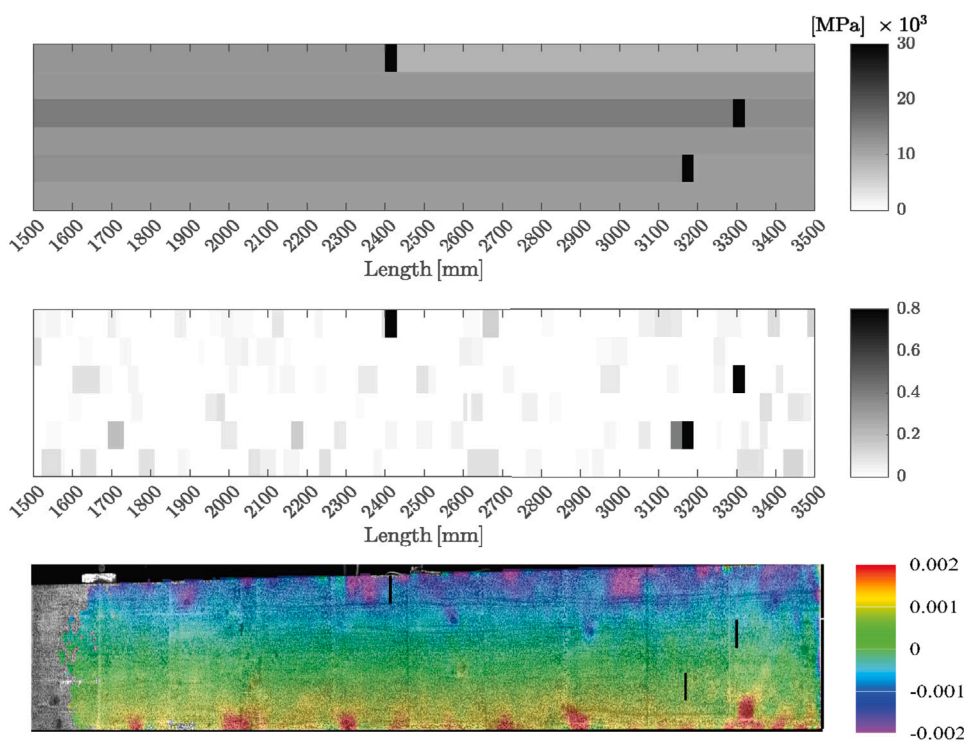

Fig. 13. E_{dyn} (top), KAR_{10} values (middle), and ε_{xx} (bottom) in the region of interest in beam no. 2. Black lines indicate the FJs.

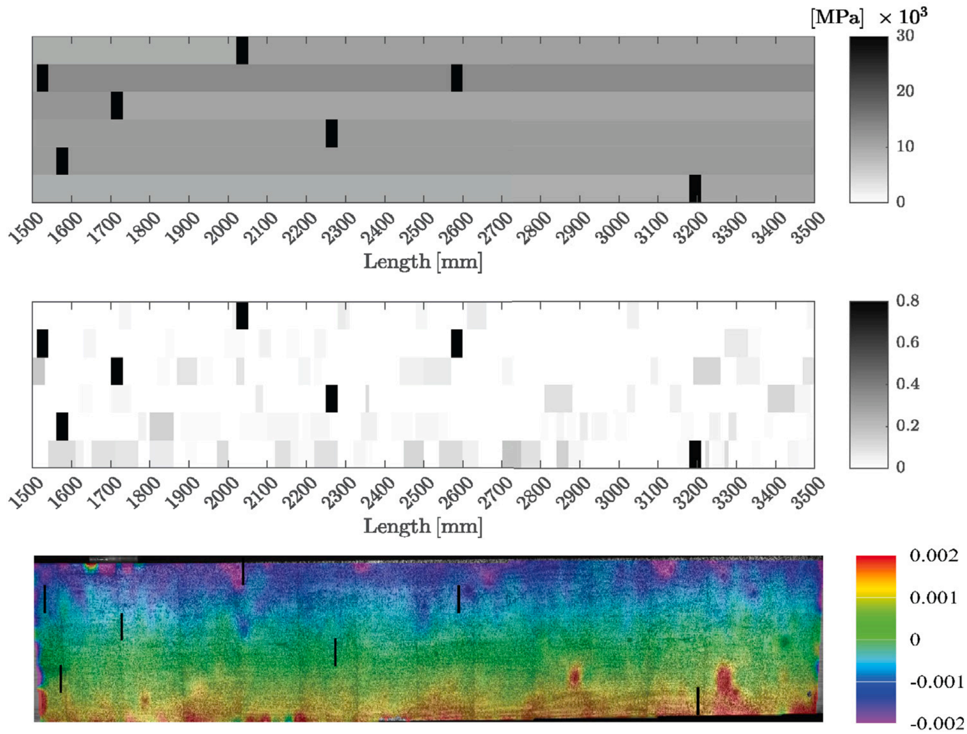

Fig. 14. E_{dyn} (top), KAR_{10} values (middle), and ε_{xx} (bottom) in the region of interest in beam no. 3. Black lines indicate the FJs.

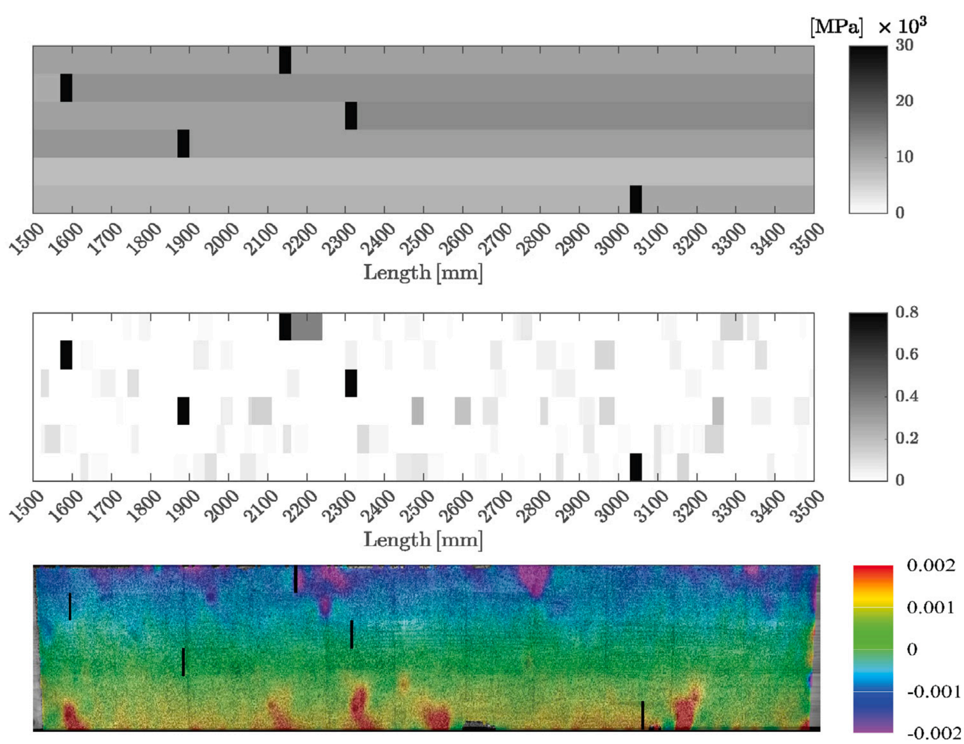

Fig. 15. E_{dyn} (top), KAR_{10} values (middle), and ε_{xx} (bottom) in the region of interest in beam no. 4. Black lines indicate the FJs.

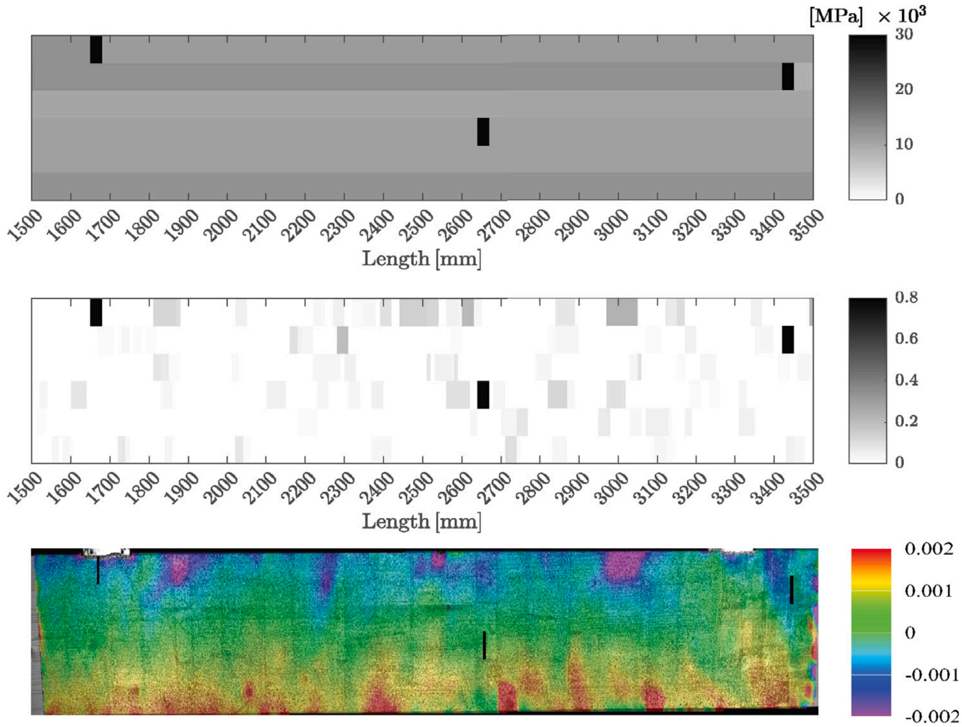

Fig. 16. E_{dyn} (top), KAR_{10} values (middle), and ε_{xx} (bottom) in the region of interest in beam no. 5. Black lines indicate the FJs.

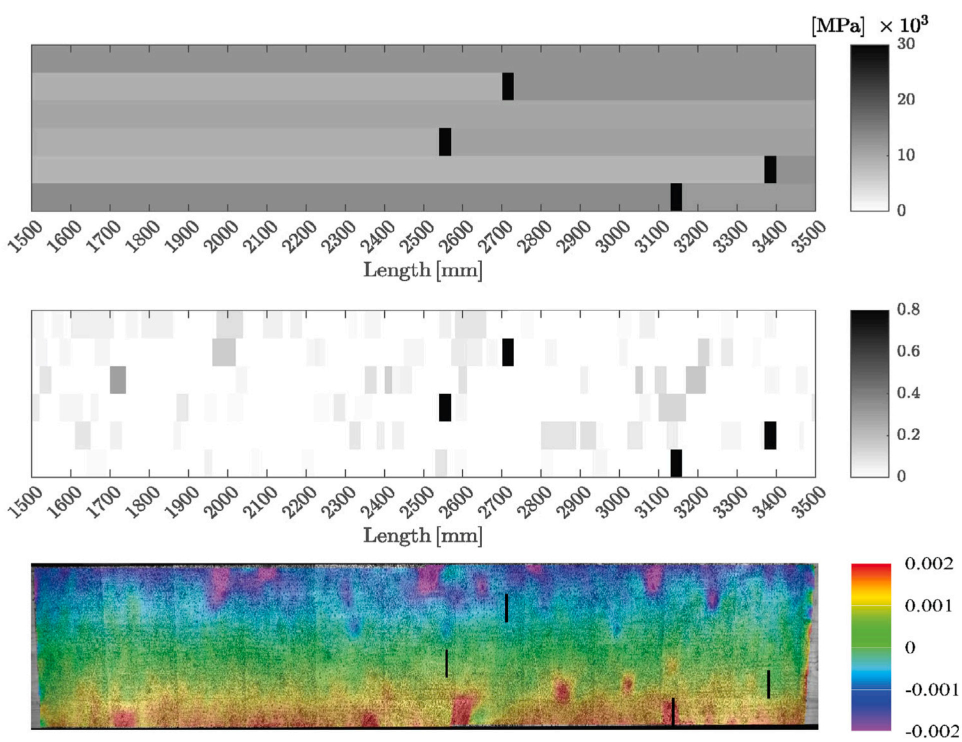

Fig. 17. E_{dyn} (top), KAR_{10} values (middle), and ε_{xx} (bottom) in the region of interest in beam no. 6. Black lines indicate the FJs.

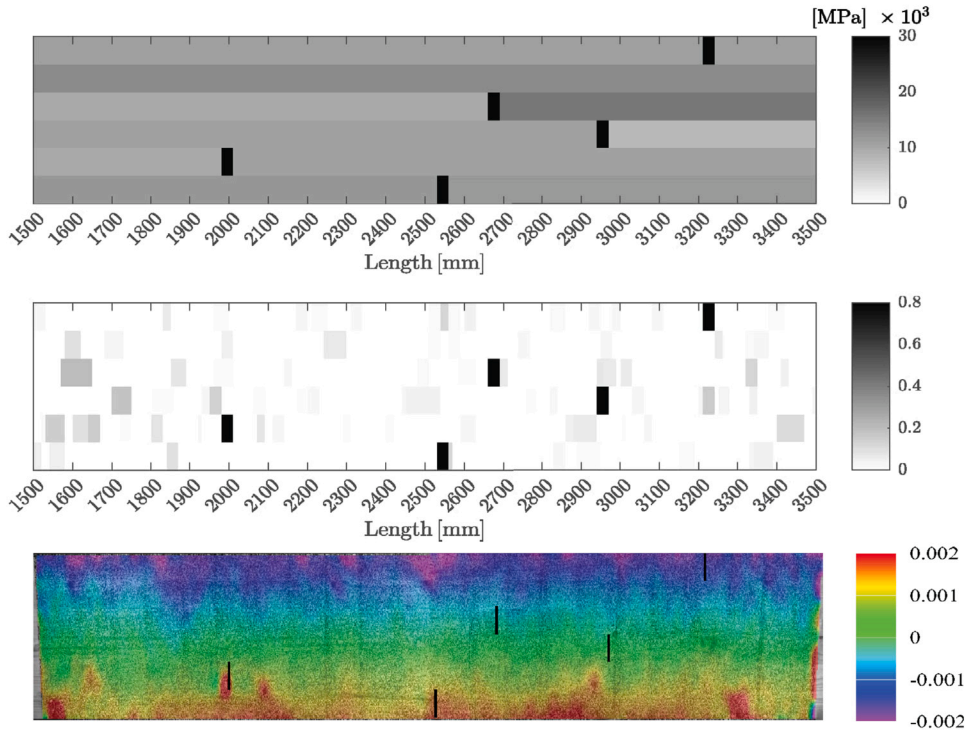

Fig. 18. E_{dyn} (top), KAR_{10} values (middle), and ε_{xx} (bottom) in the region of interest in beam no. 7. Black lines indicate the FJs.

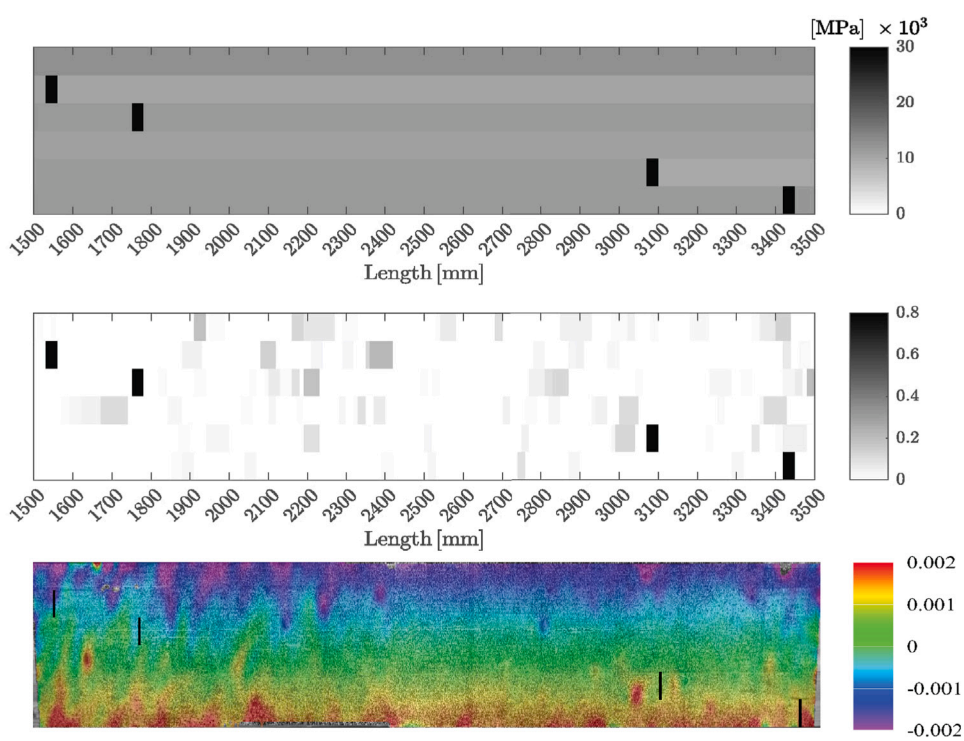

Fig. 19. E_{dyn} (top), KAR_{10} values (middle), and ε_{xx} (bottom) in the region of interest in beam no. 8. Black lines indicate the FJs.

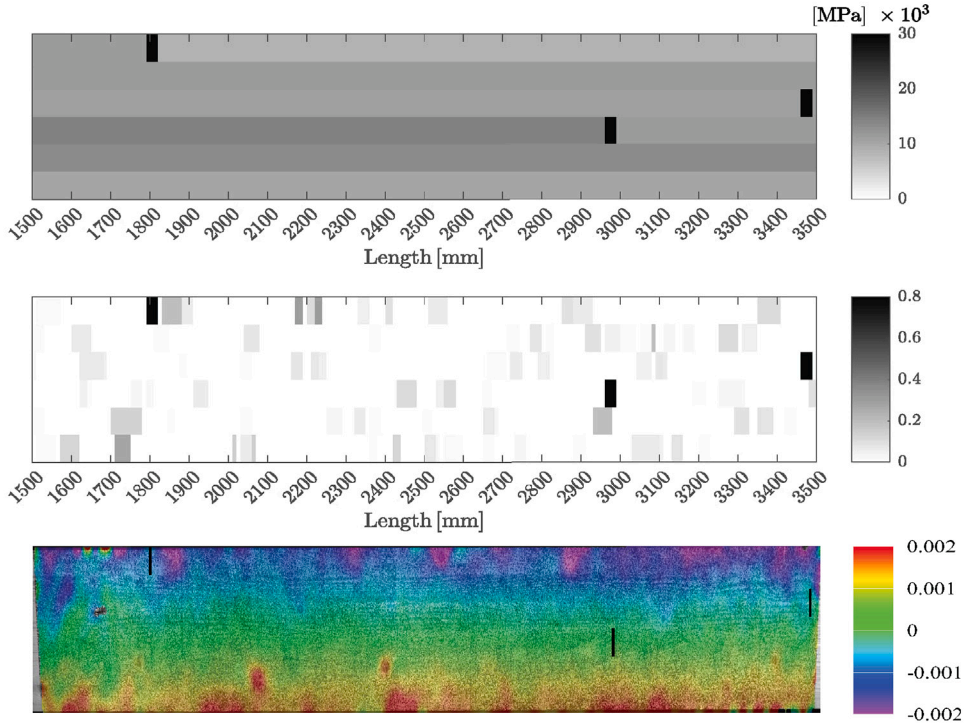

Fig. 20. E_{dyn} (top), KAR_{10} values (middle), and ε_{xx} (bottom) in the region of interest in beam no. 9. Black lines indicate the FJs.

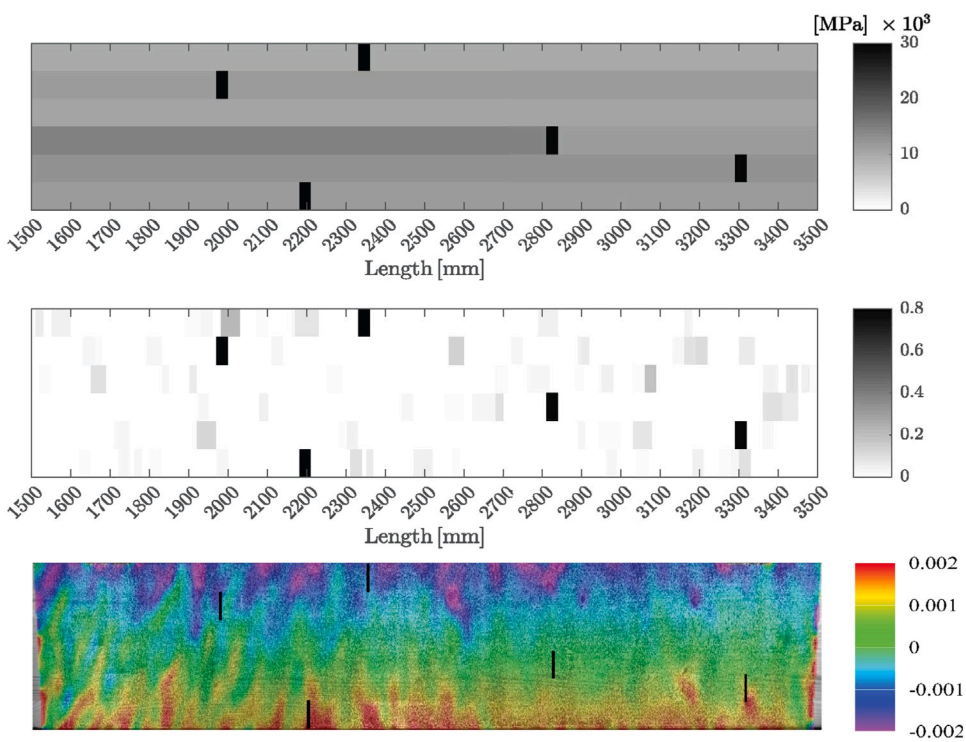

Fig. 21. E_{dyn} (top), KAR_{10} values (middle), and ε_{xx} (bottom) in the region of interest in beam no. 10. Black lines indicate the FJs.

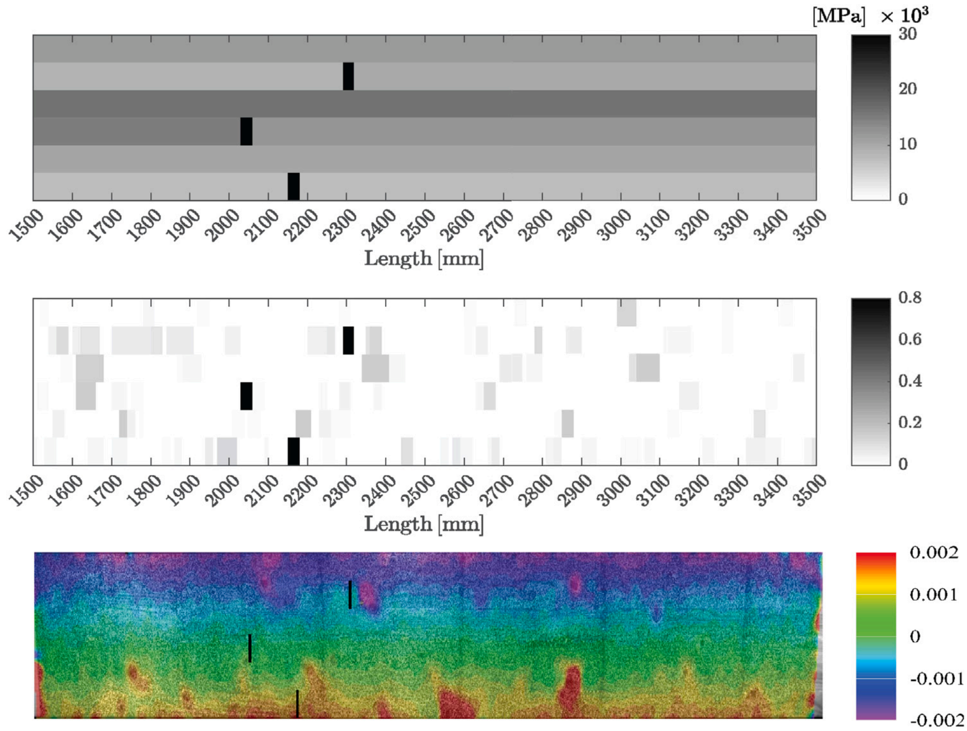

Fig. 22. E_{dyn} (top), KAR_{10} values (middle), and ε_{xx} (bottom) in the region of interest in beam no. 11. Black lines indicate the FJs.

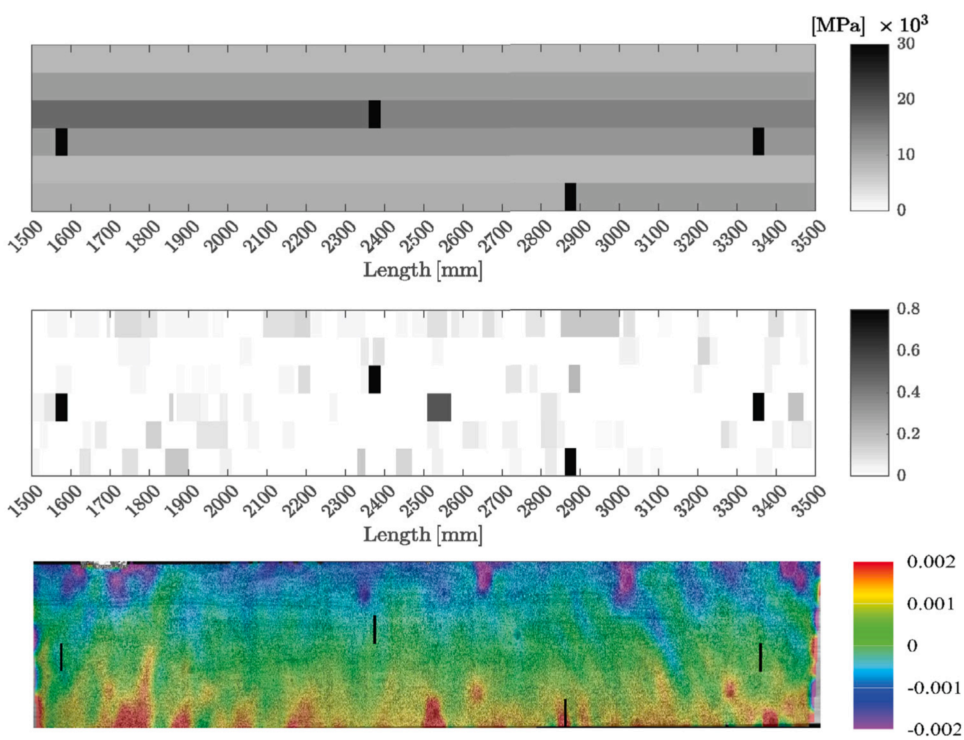

Fig. 23. E_{dyn} (top), KAR_{10} values (middle), and ε_{xx} (bottom) in the region of interest in beam no. 13. Black lines indicate the FJs.

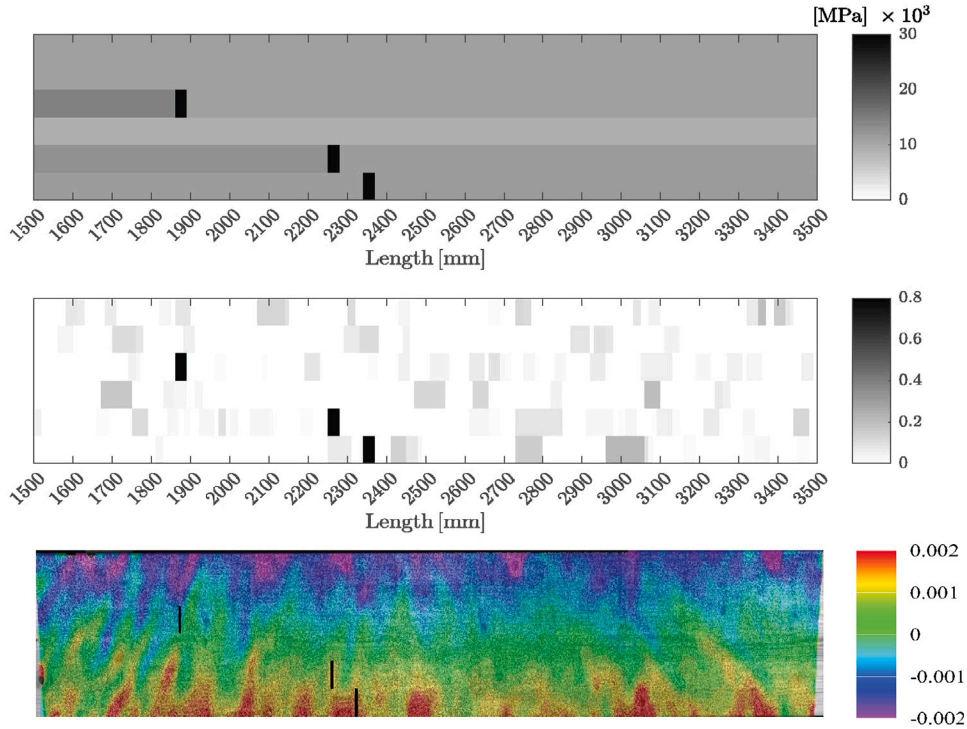

Fig. 24. E_{dyn} (top), KAR_{10} values (middle), and ε_{xx} (bottom) in the region of interest in beam no. 14. Black lines indicate the FJs.

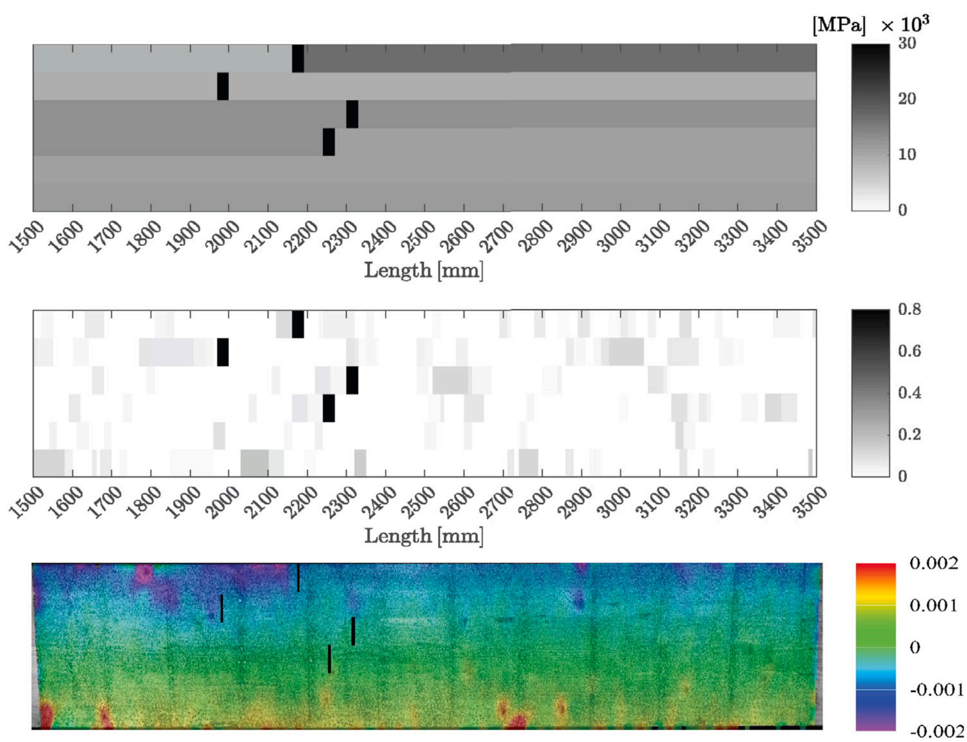

Fig. 25. E_{dyn} (top), KAR_{10} values (middle), and ε_{xx} (bottom) in the region of interest in beam no. 15. Black lines indicate the FJs.

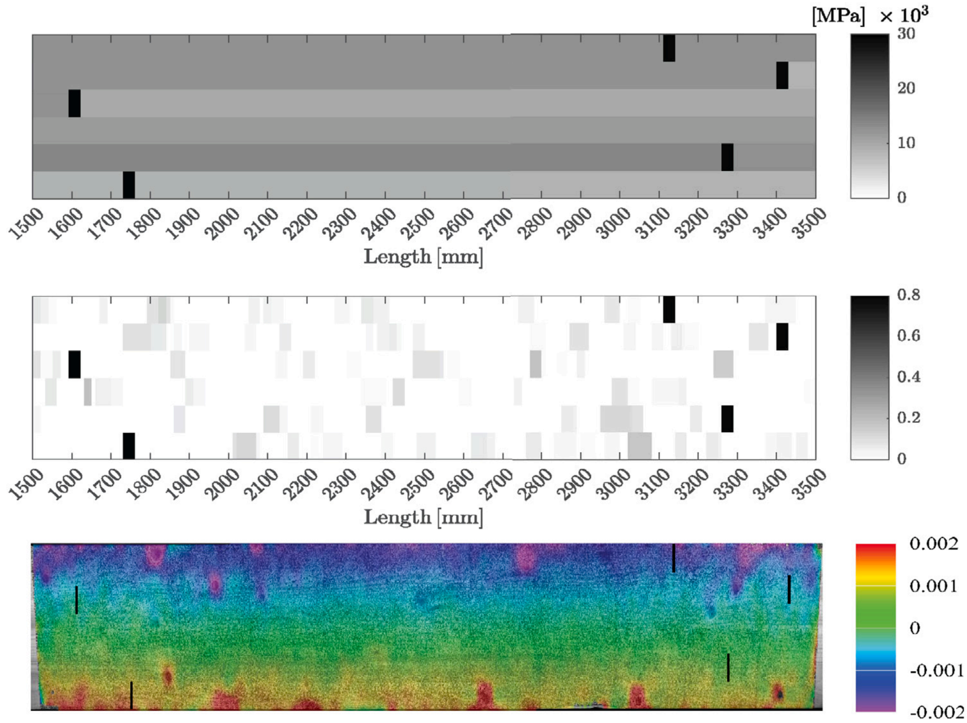

Fig. 26. E_{dyn} (top), KAR_{10} values (middle), and ε_{xx} (bottom) in the region of interest in beam no. 16. Black lines indicate the FJs.

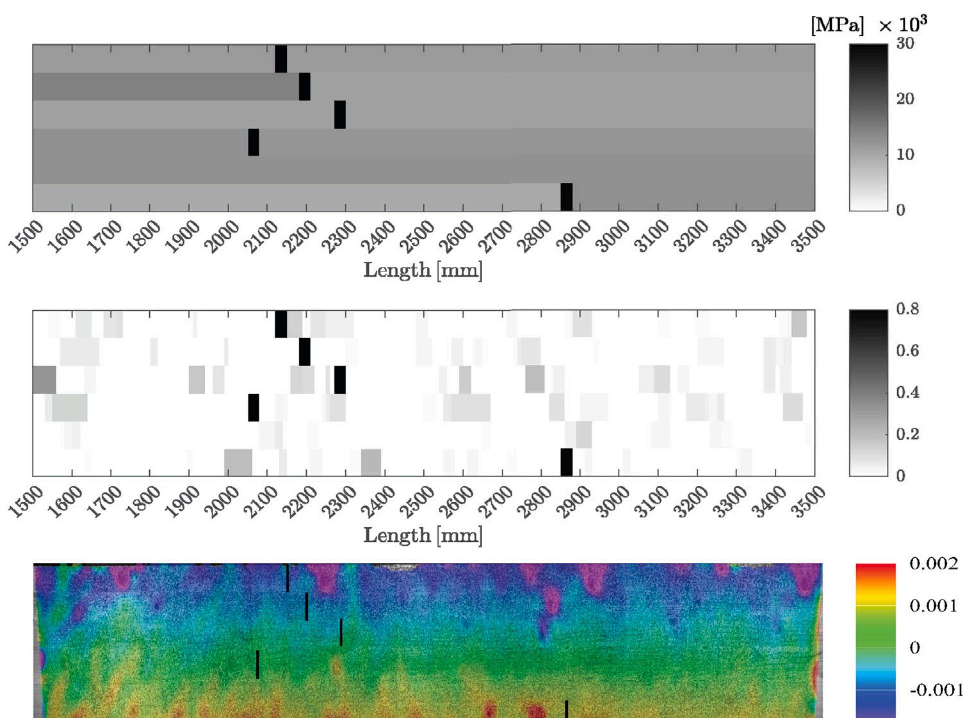

Fig. 27. E_{dyn} (top), KAR_{10} values (middle), and ε_{xx} (bottom) in the region of interest in beam no. 18. Black lines indicate the FJs.

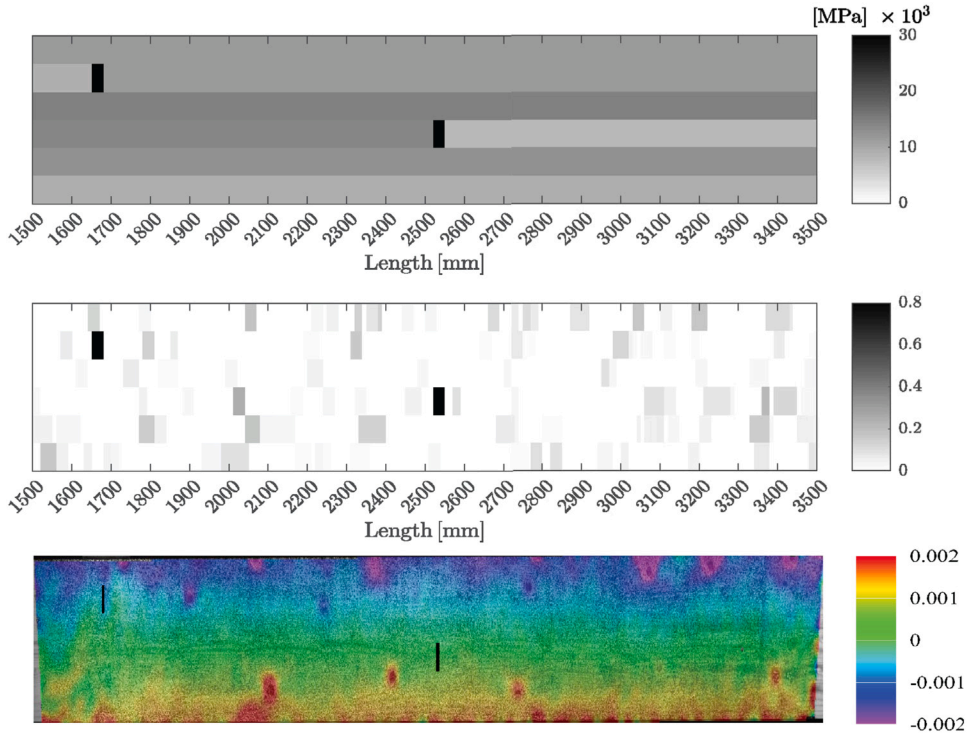

Fig. 28. E_{dyn} (top), KAR_{10} values (middle), and ε_{xx} (bottom) in the region of interest in beam no. 19. Black lines indicate the FJs.

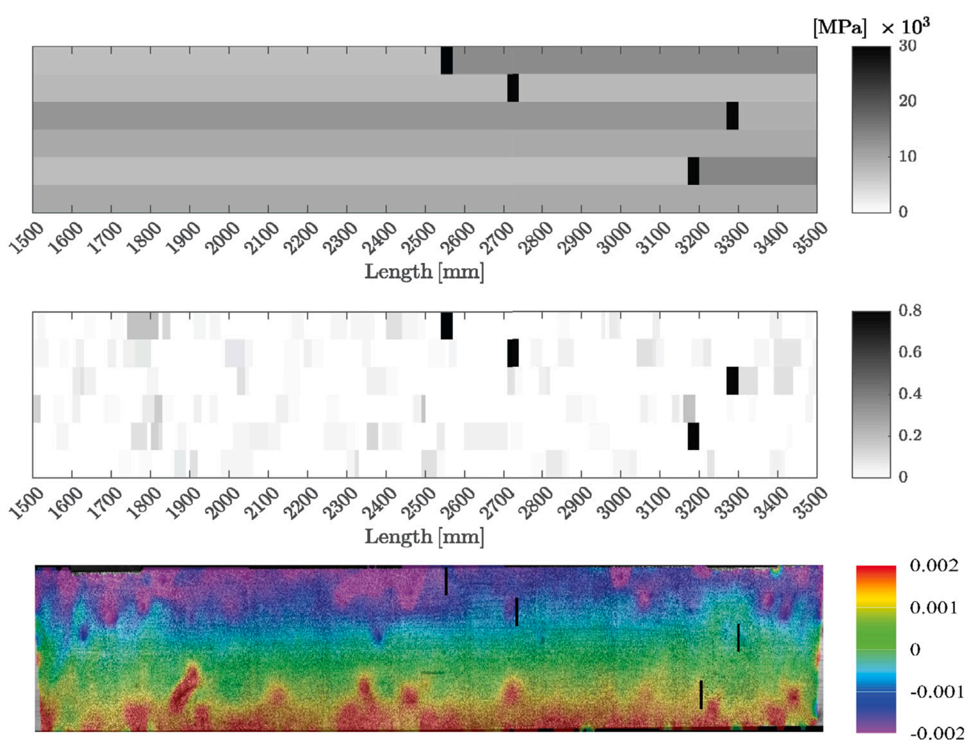

Fig. 29. E_{dyn} (top), KAR_{10} values (middle), and ε_{xx} (bottom) in the region of interest in beam no. 20. Black lines indicate the FJs.

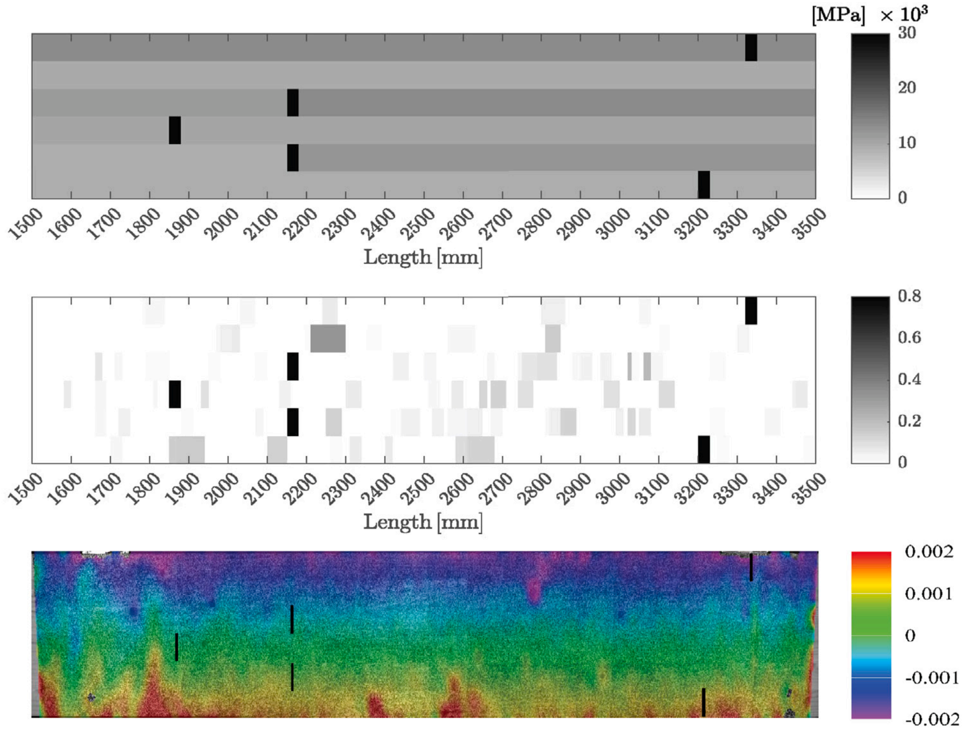

Fig. 30. E_{dyn} (top), KAR_{10} values (middle), and ε_{xx} (bottom) in the region of interest in beam no. 21. Black lines indicate the FJs.

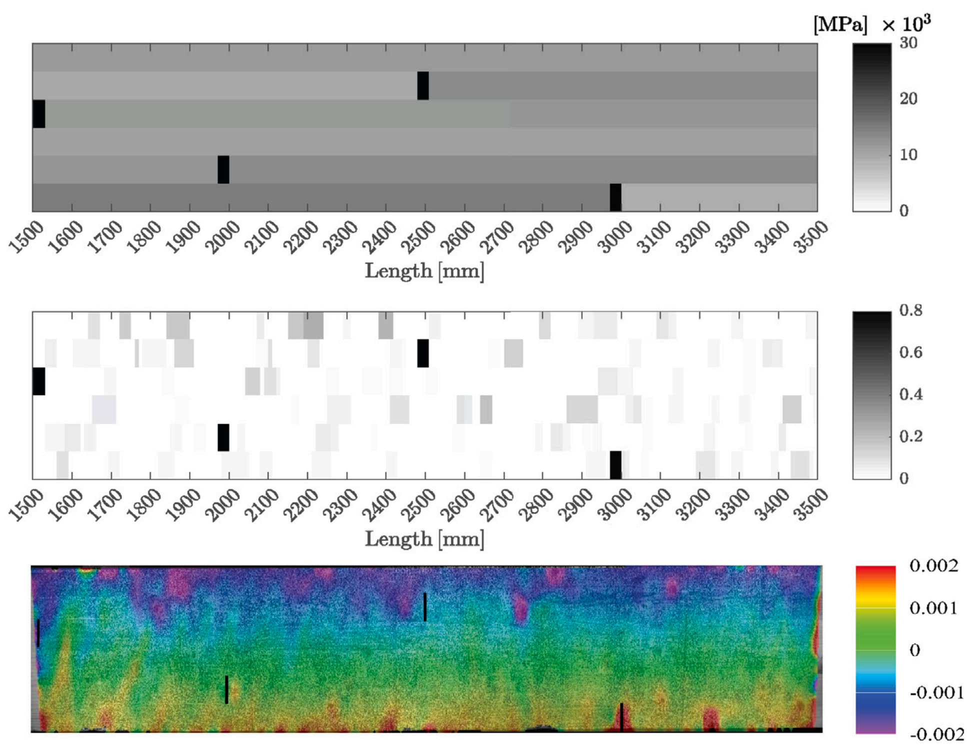

Fig. 31. E_{dyn} (top), KAR_{10} values (middle), and ε_{xx} (bottom) in the region of interest in beam no. 22. Black lines indicate the FJs.

References

[1] S. Thelandersson, H. Larsen, Timber Engineering, John Wiley & Sons, 2003.

[2] R. Brandner, G. Schickhofer, Glued laminated timber in bending: New aspects concerning modelling, Wood Sci. Technol. 42 (2008) 401–425, http://dx.doi.org/10.1007/s00226-008-0189-2.

[3] G. Fink, A. Frangi, J. Kohler, Bending tests on GLT beams having well-known local material properties, Mater. Struct. 48 (11) (2015) 3571–3584, http://dx.doi.org/10.1617/s11527-014-0424-2.

[4] G. Kandler, M. Lukacevic, J. Füssl, Experimental study on glued laminated timber beams with well-known knot morphology, Eur. J. Wood Wood Prod. 76 (2018) 1435–1452, http://dx.doi.org/10.1007/s00107-018-1328-6.

[5] G. Fink, P. Stadelmann, A. Frangi, Bending test on large-scale GLT beams with well-known beam setup using machine grading indicator, Int. Wood Prod. J. 12

(4) (2021) http://dx.doi.org/10.1080/20426445.2021.1969166.
[6] R.H. Falk, F. Colling, Laminating effects in glued-laminated timber beams, J. Struct. Eng. 121 (12) (1995) 1857–1863, http://dx.doi.org/10.1061/(ASCE)0733-9445(1995)121:12(1857).
[7] E. Serrano, H.J. Larsen, Numerical investigations of the laminating Effect in laminated beams, J. Struct. Eng. 125 (7) (1999) http://dx.doi.org/10.1061/(ASCE)0733-9445(1999)125:7(740).
[8] E. Serrano, J. Gustafsson, H.J. Larsen, Modeling of finger-joint failure in glued-laminated timber beams, J. Struct. Eng. 127 (8) (2001) 914–921, http://dx.doi.org/10.1061/(ASCE)0733-9445(2001)127:8(914).
[9] B. Heimeshoff, P. Glos, Zugfestigkeit und Biege-E-Modul von Fichten-Brettlamellen, Holz als Roh - und Werkstoff 38 (1980) http://dx.doi.org/10.1007/BF02625304.
[10] H.J. Larsen, Strength of finger-joint, in: C.F.L. Prins (Ed.), Production, Marketing and Use of Finger-Jointed Sawnwood: Proceedings of an International Seminar Organized By the Timber Committee of the United Nations Economic Commission for Europe, Hamar, Norway, at the Invitation of the Government of Norway, 15 to 19 September 1980, Springer Netherlands, Dordrecht, 1982, pp. 190–201, http://dx.doi.org/10.1007/978-94-015-3859-6_20.
[11] R. Görlacher, F. Colling, J. Ehlbeck, Glued Laminated Timber—Contribution to the Determination of the Bending Strength of Glulam Beams, International Council for Building Research Studies and Documentation - Working Commission W18 - Timber Structures, Oxford, United Kingdom, 1991.
[12] G. Fink, P. Stadelmann, A. Frangi, Tensile capacity of finger joint connections - considering censored data, in: World Conference on Timber Engineering, WCTE, 2018.
[13] F. Vafadar, S. Collins, G. Fink, Experimental investigation of finger joints under tensile and bending loads, in: World Conference on Timber Engineering, WCTE, 2023, http://dx.doi.org/10.52202/069179-0091.
[14] R.C. Moody, Tensile Strength of Finger Joints in Pith-Associated and Non-Pith-Associated Southern Pine 2 by 6's. Research Paper FPL138, U.S. Department of Agriculture Forest Service. Forest Products Laboratory (FPL), Madison, WI, 1970, URL https://api.semanticscholar.org/CorpusID:136496259.
[15] M. Samson, Potential of finger-joined lumber for machine stress-rated lumber grades, Forest Prod. J. 35 (1985) 20–24.
[16] C. Timbolmas, F.J. Rescalvo, M. Portela, R. Bravo, Analysis of poplar timber finger joints by means of Digital Image Correlation (DIC) and finite element simulation subjected to tension loading, Eur. J. Wood Wood Prod. 80 (2022) 555–567, http://dx.doi.org/10.1007/s00107-022-01806-6.
[17] J. Ehlbeck, F. Colling, R. Görlacher, Einfluß keilgezinkter Lamellen auf die Biegefestigkeit von Brettschichtholzträgern, Holz als Roh- und Werkstoff 43 (1985) 369–373.
[18] A.G. Burk, D.A. Bender, Simulating finger-joint performance based on localized constituent lumber properties, Forest Prod. J. 39 (1989) 45–50, URL https://api.semanticscholar.org/CorpusID:222242014.
[19] G. Fink, Influence of Varying Material Properties on the Load-Bearing Capacity of Glued Laminated Timber (Ph.D. thesis), ETH Zurich, 2014.
[20] J. Oscarsson, A. Olsson, B. Enquist, Strain fields around a traversing edge knot in a spruce specimen exposed to tensile forces, in: World Conference on Timber Engineering, WCTE, 2010.
[21] H. Nagai, K. Murata, T. Nakano, Strain analysis of lumber containing a knot during tensile failure, J. Wood Sci. 57 (2011) 114–118, http://dx.doi.org/10.1007/s10086-010-1154-x.
[22] G. Fink, J. Kohler, A. Frangi, Experimental analysis of the deformation and failure behaviour of significant knot clusters, in: World Conference on Timber Engineering, WCTE, 2012.
[23] C.W. Chang, F.C. Lin, Strain concentration effects of wood knots under longitudinal tension obtained through digital image correlation, Biosyst. Eng. 212 (2021) 290–301, http://dx.doi.org/10.1016/j.biosystemseng.2021.10.014.
[24] Dynalyse AB, precigrader, strength grading timber machine, 2023, URL https://dynalyse.com/products/strength-grading-lumber-timber/precigrader/.
[25] Microtec, finscan, visual timber scanning machine, 2023, URL https://www.microtec.eu/en/products/finscan.
[26] SFS-EN 338: Structural Timber. Strength Classes, Standard, Finnish Standards Association, Helsinki, 2010.
[27] T. Isaksson, Modelling the Variability of Bending Strength in Structural Timber - Length and Load Configuration Effects (Ph.D. thesis), Lund University, 1999.
[28] SFS-EN 15497: Structural Finger Jointed Solid Timber. Performance Requirements and Minimum Production Requirements, Standard, Finnish Standards Association, Helsinki, 2014.
[29] SFS-EN 408 + A1: Timber structures. Structural Timber and Glued Laminated Timber. Determination of Some Physical and Mechanical Properties, Standard, Finnish Standards Association, Helsinki, 2012.
[30] E.M.C. Jones, M.A. Iadicola (Eds.), A Good Practices Guide for Digital Image Correlation, International Digital Image Correlation Society (iDICs), 2018, p. 94, URL http://idics.org/guide/.
[31] A. Forsström, S. Bossuyt, G. Scotti, H. Hänninen, Quantifying the effectiveness of eatterning, test conditions, and DIC parameters for characterization of plastic strain localization, Exp. Mech. 60 (1) (2019) 3–12, http://dx.doi.org/10.1007/s11340-019-00510-6.
[32] S. Bossuyt, Optimized patterns for digital image correlation, in: H. Jin, C. Sciammarella, C. Furlong, S. Yoshida (Eds.), Imaging Methods for Novel Materials and Challenging Applications, Springer New York, New York, 2013, pp. 239–248.
[33] S. Collins, G. Fink, Mechanical behaviour of sawn timber of silver birch under compression loading, Wood Mater. Sci. Eng. 17 (2) (2020) 121–128, http://dx.doi.org/10.1080/17480272.2020.1801836.
[34] Correlated solutions, inc., VIC-snap image acquisition software (Version 9, build 3604), 2021.
[35] Correlated solutions, inc., VIC-3D digital image correlation software (Version 9.4.26), 2022.
[36] SFS-EN 14080: Timber Structures. Glued Laminated Timber and Glued Solid Timber. Requirements, Standard, Finnish Standards Association, Helsinki, 2013.
[37] Joint Community on Structural Safety, Part 3: Resistance Models–3.5 Properties of Timber, Tech. Rep., 2006, Probabilistic Model Code. Joint Committee on Structural Safety.
[38] G. Fink, R. Brandner, P. Palma, J. Kohler, Volume effects in glued laminated timber beams, in: 14th International Conference on Applications of Statistics and Probability in Civil Engineering, ICASP14, Dublin, 2023.